

Relativistic Orbital Optimized Density Functional Theory for Accurate Core-Level Spectroscopy

Leonardo A. Cunha,^{*,†,‡,§} Diptarka Hait,^{*,†,‡,§} Richard Kang,^{†,‡} Yuezhi Mao,[¶] and
Martin Head-Gordon^{*,†,‡}

[†]*Kenneth S. Pitzer Center for Theoretical Chemistry, Department of Chemistry, University
of California, Berkeley, California 94720, USA*

[‡]*Chemical Sciences Division, Lawrence Berkeley National Laboratory, Berkeley, California
94720, USA*

[¶]*Department of Chemistry, Stanford University, Stanford, CA 94305, USA*

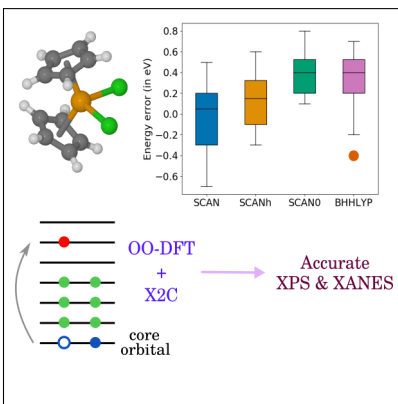
[§]*These authors contributed equally to this work.*

E-mail: leonardo.cunha@berkeley.edu; diptarka@berkeley.edu; mhg@cchem.berkeley.edu

Abstract

Core-level spectra of 1s electrons of elements heavier than Ne show significant relativistic effects. We combine advances in orbital optimized DFT (OO-DFT) with the spin-free exact two-component (X2C) model for scalar relativistic effects, to study K-edge spectra of third period elements. OO-DFT/X2C is found to be quite accurate at predicting energies, yielding ~ 0.5 eV RMS error vs experiment with the modern SCAN (and related) functionals. This marks a significant improvement over the > 50 eV deviations that are typical for the popular time-dependent DFT (TDDFT) approach. Consequently, experimental spectra are quite well reproduced by OO-DFT/X2C, sans empirical shifts for alignment. OO-DFT/X2C combines high accuracy with ground state DFT cost and is thus a promising route for computing core-level spectra of third period elements. We also explored K and L edges of 3d transition metals to identify limitations of the OO-DFT/X2C approach in modeling the spectra of heavier atoms.

Graphical TOC Entry



Spectroscopy of core-level electrons with X-rays is a convenient and popular tool for studying chemical systems. A specific core-level of a given element normally has a characteristic energy that is quite distinct from inner-shells of other elements, making the technique element specific. Furthermore, core electrons do not play a direct role in chemical bonding, and are thus effectively localized around the nucleus. Spectroscopic probe of these electrons therefore yields information about local chemical environment of individual atoms. Core-level spectra can thus yield useful information about the local coordination environment,^{1,2} extent of covalency in ligand-metal interactions^{3,4} or the oxidation state.⁵ Time-resolved core-level spectroscopy can also be used as a probe to study photoinduced chemical dynamics.⁶⁻⁸

Computational simulations of core-level spectra are useful for gaining insight into experiment, and potentially identifying new species whose signature may appear in transient spectra.⁸⁻¹⁰ Traditional quantum chemistry methods for excited states^{11,12} are however quite challenged by this task, especially since such techniques are mostly developed for (and validated on) problems involving only valence electrons. For example, the widely used linear-response time-dependent density functional theory (TDDFT) approach^{11,13} cannot adequately describe the relaxation of the core hole. This leads to rather large errors of ~ 10 - 20 eV for the K-edge (1s orbitals) of C, N, O and F,^{10,14-18} if highly specialized functionals^{19,20} are not employed. Heavier elements lead to even larger errors, such as ~ 50 eV for the P, S, Cl K-edges²¹⁻²³ and > 100 eV for the Fe K-edge.²⁴ TDDFT spectra therefore usually need to be empirically translated by many eVs, in order to align with experiment.^{10,22,24,25} Similar behavior is observed for the equation-of-motion coupled cluster singles and doubles (EOM-CCSD) method,^{12,26} although the shift required is typically much smaller (< 2 eV for second period elements).²⁷⁻³¹ EOM-CCSD is however quite computationally demanding, with the computational cost scaling as $O(N^6)$ vs system size N (compared to $O(N^{3-4})$ for DFT).

Orbital-optimized (OO) methods optimize orbitals for each excited state individually, and separately from those of the ground state. OO can therefore effectively model the relaxation of the core hole, leading to much better agreement with experiment³²⁻³⁵ without any need

for empirical shifts. Unfortunately, OO methods had been historically underutilized due to a risk of ‘variational collapse’, in which the calculation converges to a lower energy state (often the ground state) instead of the desired high energy excitation. However, there has been considerable recent interest in excited state OO, resulting in many new approaches that aim to reliably converge to any chosen state without the risk of variational collapse.^{36–42} In practice, OO-DFT methods require more compute time than TDDFT if a large number of states are desired, such as in (near-)degenerate bands. This stems from OO-DFT having to iteratively optimize multiple states individually while TDDFT can simultaneously compute them. However, OO-DFT retains the same computational scaling as ground state DFT or TDDFT. An overview of the successes and challenges with OO-DFT methods can be found in Ref 33. OO-DFT methods are thus increasingly being employed to study core-level spectra,^{40,43–47} with the modern SCAN⁴⁸ functional leading to very low error^{43,44,47,49} (< 1 eV) vs experiment for the K-edge of C, N, O and F, as well as L-edges of Si, P, S and Cl.

The K-edge of elements heavier than F however cannot be as accurately modeled with non-relativistic quantum mechanics. Naive use of the Bohr atom model suggests that the speed of 1s electrons would scale linearly with the atomic number Z , eventually attaining the speed of light at $Z > \alpha^{-1} \approx 137$ (where α is the fine structure constant). Relativistic effects become perceptible at much smaller Z , with calculations indicating that non-relativistic quantum mechanics underbinds the 1s electrons of Ne by 1 eV.⁵⁰ It is therefore necessary to incorporate relativistic effects into OO-DFT, if < 1 eV error vs experiment is desired for computed K-edge spectra of third period elements and beyond. Scalar relativistic treatment is however often overlooked for linear-response TDDFT, as the ad-hoc empirical shifts (typically larger than the relativistic correction) utilized to align computation with experiment account for it to some extent.^{51–53} Nonetheless, explicit use of relativistic effects in TDDFT has been previously explored, albeit mostly within a real-time framework.^{15,53,54} Similarly, both empirical shifts²⁸ and explicit inclusion^{55,56} have been used to account for relativistic effects in coupled cluster methods. The use of element-specific corrections to nonrelativistic

TDDFT results has also been examined in the past.¹⁹

In this work, we utilize the spin-free exact-two component one electron (SFX2C-1e, henceforth referred to as just X2C) model for relativistic quantum chemistry⁵⁷⁻⁶⁴ to obtain improved OO-DFT core-level spectra. The X2C model transforms the one particle terms of the electronic Hamiltonian (i.e. kinetic energy and external potential) via the solutions of the four component, one electron Dirac Hamiltonian. The two-particle (i.e. interelectron interaction) terms are treated within the pure Coulomb formalism and, therefore, are left unaltered in the non-relativistic form, permitting straightforward application of DFT. The transformation is briefly described in the supporting information, and we invite interested readers to examine Refs. 61 and 62 for further details regarding X2C.

Using the X2C transformed one particle Hamiltonian, we obtained the ground state energy via the standard Kohn-Sham⁶⁵ (KS) formalism. Excited states are more challenging, as many excitations unpair electrons and therefore require multiple Slater determinants for a spin-pure description. DFT for such states is not straightforward, as the KS-DFT formalism with existing density functional approximations can only be reliably applied to single-reference systems. We therefore utilize three related OO-DFT ansatze for modeling three classes of excited states. These ansatze are described in detail in Ref 33, but we provide a brief outline here for convenience.

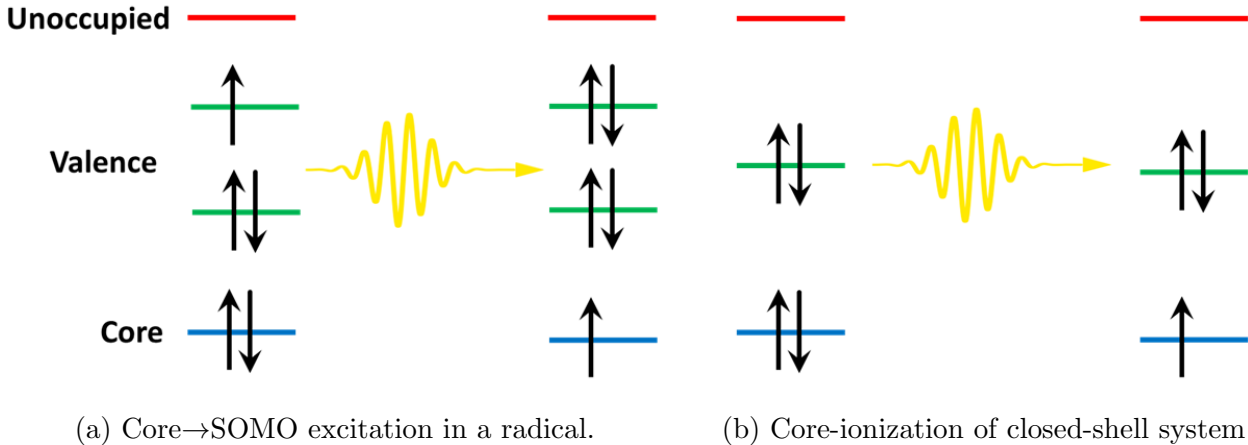


Figure 1: Schematic for processes where Δ SCF is appropriate.

A state with no unpaired electrons, or one with all unpaired electrons of the same spin can be represented by a single Slater determinant. It is straightforward to optimize a single Slater determinant with an excited state electronic configuration (apart from the aforementioned risk of variational collapse). This protocol is called Δ SCF^{66,67} and is suitable for states that result from $1s \rightarrow$ SOMO (singly occupied molecular orbital) transitions of open-shell species, or core-ionized states of closed-shell molecules (as shown in Fig 1). Relativistic Δ Hartree-Fock (HF) has indeed been used to study core-ionization energies^{68,69}. However, Δ SCF is not appropriate for singly excited singlet excited states of closed-shell molecules, as both the up and down spins are equally likely to be excited (as shown in Fig 2). Exciting only one spin results in a spin-contaminated determinant midway between singlet and triplet. Spin-contaminated Δ SCF energies have nonetheless been utilized in the past for core-excitation energy calculations, with element-specific relativistic corrections for heavy elements.³²

Restricted open-shell Kohn-Sham^{70,71} (ROKS) obtains a pure singlet energy by spin-projection on the spin-contaminated determinant. ROKS is consequently the optimal OO-DFT approach for singlet excited states with two unpaired spins, although it cannot be applied if there are more than two unpaired spins. Such states require a more general recoupling scheme described in Refs 33 and 44. This is however only necessary for transitions from the core to completely unoccupied levels in open-shell systems, with Δ SCF and ROKS being sufficient for all the states considered in this work. OO-DFT therefore encompasses Δ SCF and methods like ROKS and the general recoupling scheme that derive from it.

We first examined the performance of OO-DFT/X2C in predicting the gas phase K-edge spectra of the third period elements (and Ne) with Table 1 reporting Δ SCF $1s$ electron binding energies for several closed-shell species. All presented functionals have root mean square error (RMSE) < 1 eV vs experimental X-ray photoelectron spectra (XPS). These functionals were identified via screening across many functionals over a smaller set of species ($\text{SiH}_4, \text{PH}_3, \text{H}_2\text{S}, \text{HCl}$ and Ar). This screening also revealed that other well known functionals like B3LYP,^{85,86} PBE0,⁸⁷ or TPSS⁸⁸ have larger errors ($\sim 1-3$ eV, as shown in the sup-

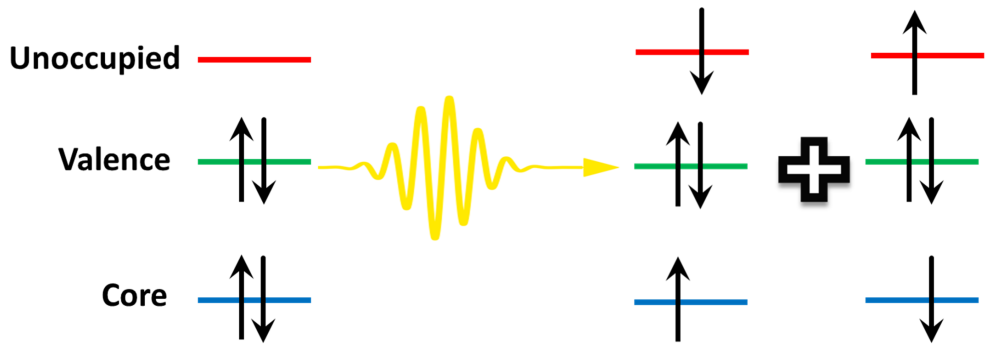


Figure 2: Schematic for a singlet core excitation in a closed-shell species. Two open-shell determinants (as seen on the right) are equally likely, and are individually halfway between singlet and triplet in character. ROKS is thus essential for spin-purity of the excited state.

porting information) that nonetheless represent a major improvement over TDDFT or non-relativistic OO-DFT. Out of the selected functionals, SCAN fares particularly well, yielding an RMSE of 0.4 eV and a maximum deviation of 0.8 eV from experiment. X2C is crucial for this level of agreement, as SCAN with the non-relativistic (NR) Hamiltonian leads to errors of several eV (as shown in Table 1). The related SCANh⁸⁹ functional performs slightly worse, but is still fairly accurate. SCANh does have positive mean error (ME), indicating it systematically overestimates the binding energy. This overestimation is a consequence of the presence of HF exchange (10%) in the functional, as pure HF overestimates by ~ 2 eV. Overestimation is more evident for SCAN0⁹⁰ (which has 25% HF exchange) and BHHLYP⁹¹ (50% HF exchange). However, it is important to note that the ME is strongly influenced by the choice of the local exchange-correlation model. For example, functionals based on PBE⁹² appear to be far more sensitive to % HF exchange, than ones derived from SCAN (as seen in the supporting information). In addition, most local functionals strongly underbind core-electrons, and would require admixture of a very large amount of % HF exchange to have low error (BHHLYP being a prominent example). SCAN is a notable exception in this regard, as it has low error despite being a local functional.

We next considered prediction of X-ray absorption spectra (XAS) with ROKS, which is quite effective in predicting singlet core excitation energies of second period elements.⁴³

Table 1: Gas phase XPS K-edge binding energies for Ne and third period elements (in eV). Computed values were found from restricted open-shell Δ SCF calculations, using the aug-pcX-2 basis⁸³ when available and decontracted aug-pcseg-2⁸⁴ for H/Br. Non-relativistic (NR) values from SCAN are also provided for comparison. The root mean square error (RMSE), mean error (ME) and maximum absolute error (MAX) are also reported. The atomic site of the ionization is bolded when multiple possibilities exist.

Molecule	Expt.	SCAN (NR)	SCAN	SCANh	SCAN0	BHHLYP	HF
Ne	870.2 ⁷²	869.3	870.3	870.3	870.3	870.5	869.6
Mg	1311.5 ⁷³	1309.3	1311.6	1311.6	1311.6	1311.5	1311.4
SiH ₄	1847.0 ⁷⁴	1842.7	1847.1	1847.2	1847.3	1847.3	1848.0
SiF ₄	1852.5 ⁷⁴	1847.8	1852.1	1852.4	1852.7	1852.8	1853.7
SiCl₄	1850.6 ⁷⁴	1846.1	1850.5	1850.7	1850.9	1851.0	1852.0
SiBr ₄	1849.7 ⁷⁴	1845.5	1849.8	1850.0	1850.3	1850.3	1851.3
PH ₃	2150.9 ⁷⁵	2145.1	2151.0	2151.1	2151.2	2151.0	2152.0
PF ₃	2156.4 ⁷⁵	2150.0	2155.8	2156.1	2156.4	2156.4	2157.7
PF ₅	2159.4 ⁷⁵	2153.2	2159.0	2159.3	2159.8	2160.0	2161.6
POF ₃	2157.8 ⁷⁵	2151.7	2157.5	2157.8	2158.2	2158.4	2159.9
H ₂ S	2478.5 ⁷⁶	2470.7	2478.4	2478.6	2478.8	2478.4	2479.5
CS ₂	2478.1 ⁷⁷	2470.4	2478.2	2478.3	2478.5	2478.0	2479.1
SF ₄	2486.9 ⁷⁸	2478.7	2486.5	2486.8	2487.3	2487.4	2489.3
SF ₆	2490.1 ⁷⁶	2481.9	2489.6	2489.9	2490.5	2490.6	2492.7
SO ₂	2483.7 ⁷⁶	2475.9	2483.6	2483.9	2484.3	2484.2	2486.0
CSO	2478.7 ⁷⁷	2471.2	2479.0	2479.1	2479.3	2478.8	2479.9
SF₅Cl	2488.9 ⁷⁸	2480.9	2488.6	2489.0	2489.5	2489.5	2491.5
HCl	2829.8 ⁷⁹	2820.3	2830.3	2830.4	2830.6	2830.0	2831.4
Cl ₂	2830.2 ⁷⁹	2820.8	2830.8	2831.0	2831.2	2830.5	2831.9
CH ₃ Cl	2828.4 ⁸⁰	2819.2	2829.2	2829.3	2829.5	2828.9	2830.2
SF₅Cl	2829.6 ⁸¹	2820.3	2830.4	2830.6	2830.9	2830.3	2831.8
CCl ₃ F	2829.3 ⁸⁰	2820.0	2830.0	2830.2	2830.4	2829.8	2831.2
Ar	3206.3 ⁸²	3194.1	3206.9	3207.0	3207.3	3206.5	3208.1
RMSE		7.4	0.4	0.5	0.6	0.4	1.7
ME		-6.9	0.1	0.3	0.5	0.3	1.5
MAX		12.2	0.8	1.0	1.3	0.7	2.7

Table 2 shows that inclusion of scalar relativistic effects through the X2C model permits high accuracy for third period elements as well. SCANh yields the best performance with an RMSE of 0.3 eV and a maximum absolute error (MAX) of only 0.6 eV. SCAN and SCAN0 also yield quite good performance. In fact, the RMSE for all the presented functionals is comparable to the typical experimental energy resolution of ~ 0.5 eV, and therefore

Table 2: Lowest dipole allowed gas-phase XAS excitation energy for third period elements (in eV). Computed values were found from ROKS, using the aug-pcX-2 basis when available and decontracted aug-pcseg-2 for H/Br. NR values from SCAN are also provided for comparison. The atomic site of the ionization is bolded when multiple possibilities exist.

Molecule	Expt.	SCAN (NR)	SCAN	SCANh	SCAN0	BHHLYP	HF
SiH ₄	1842.7 ⁷⁴	1838.56	1842.9	1843.1	1843.3	1843.4	1844.9
SiF ₄	1849.0 ⁷⁴	1844.13	1848.5	1848.8	1849.1	1849.4	1851.3
SiCl₄	1846.0 ⁷⁴	1841.37	1845.7	1845.9	1846.2	1846.5	1848.5
SiBr ₄	1845.0 ⁷⁴	1840.58	1844.9	1845.1	1845.4	1845.6	1847.7
PH ₃	2145.8 ⁹³	2140.15	2146.0	2146.2	2146.4	2146.3	2148.1
PF ₃	2149.3 ⁹³	2143.55	2149.4	2149.6	2149.9	2150.0	2151.9
PF ₅	2155.0 ⁹³	2148.59	2154.5	2154.7	2155.2	2155.5	2159.8
POF ₃	2153.3 ⁹³	2147.16	2153.0	2153.3	2153.7	2153.9	2158.0
H ₂ S	2472.7 ⁹⁴	2465.05	2472.8	2473.0	2473.2	2472.9	2475.0
CS ₂	2470.8 ⁷⁷	2463.53	2471.3	2471.3	2471.4	2471.0	2472.5
SF ₄	2477.3 ⁹⁵	2469.71	2477.4	2477.7	2478.0	2478.0	2480.5
SF ₆	2486.0 ⁹⁴	2477.55	2485.3	2485.7	2486.2	2486.5	2490.1
SO ₂	2473.2 ⁹⁴	2465.53	2473.3	2473.4	2473.6	2473.4	2475.5
CSO	2472.0 ⁷⁷	2464.73	2472.5	2472.6	2472.7	2472.2	2473.9
SF₅Cl	2483.5 ⁸¹	2475.11	2482.8	2483.2	2483.7	2483.9	2487.3
HCl	2823.9 ⁷⁹	2813.79	2823.8	2824.0	2824.2	2823.7	2825.7
Cl ₂	2821.3 ⁷⁹	2811.05	2821.1	2821.2	2821.4	2820.9	2822.8
CH ₃ Cl	2823.5 ⁸⁰	2813.60	2823.6	2823.8	2824.0	2823.6	2825.8
SF₅Cl	2821.8 ⁸¹	2811.83	2821.8	2821.9	2822.1	2821.6	2823.7
CCl ₃ F	2822.8 ⁸⁰	2813.19	2823.2	2823.4	2823.6	2823.2	2825.3
RMSE		7.6	0.4	0.3	0.5	0.5	2.8
ME		-7.3	-0.1	0.1	0.4	0.3	2.7
MAX		10.3	0.7	0.6	0.8	0.7	4.8

indicative of semi-quantitative performance. Curiously, SCAN significantly underestimates the excitation energy for highly fluorinated compounds (SF₆, CF₃SF₅ etc.), highlighting a potential limitation for this otherwise excellent performing local functional. This systematic underestimation is partially mitigated with HF exchange, leading to SCANh performing somewhat better. On the other hand, SCAN0 has a systematic bias towards overestimation due to a greater part of HF exchange being present. SCANh therefore offers a reasonable middle path, although it would perform poorly for cases where SCAN already overestimates or SCAN0 underestimates. We also note that our RMSEs are considerably smaller than the

several eV errors reported by an earlier study⁶⁴ using relativistic orthogonality constrained DFT (OC-DFT),⁹⁶ which may in part stem from use of B3LYP in that work.

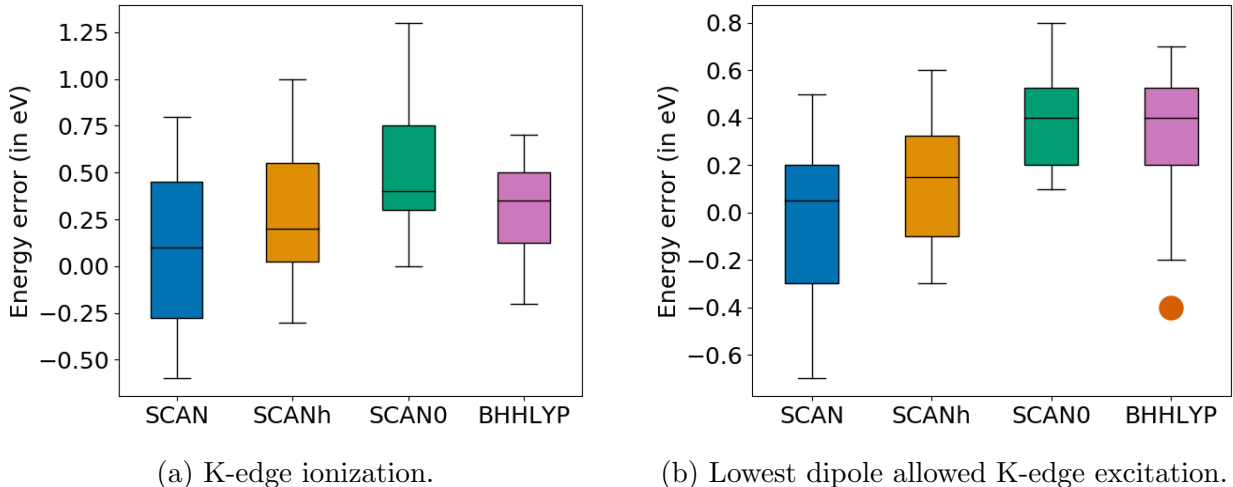


Figure 3: Box plot for errors (vs experiment) in computed values reported in Tables 1-2. The red dot in Fig. 3b represents an outlier (Cl_2) where BHLYP unusually underestimates the excitation energy by 0.4 eV.

Fig 3 visually summarizes the key result shown in Tables 1 and 2, namely that OO-DFT/X2C is effective in predicting core-level excitation/ionization energies of third period atoms in isolated small molecules. The error distributions are quite compact overall, with the typical limits being below 1 eV. In particular, the SCAN, SCANh and BHLYP functionals typically have errors below 0.5 eV, and never over 1.0 eV (for the species considered). They therefore appear to be promising routes for prediction of gas-phase core-level spectra.

It is also worthwhile to consider larger systems in order to gauge feasibility of OO-DFT/X2C for widespread practical use. However, certain computational challenges need to be considered along the way. Decontracted basis sets of at least triple- ζ quality (ideally of the Jensen pcX-n⁸³ or Dunning cc-pCVnZ⁹⁷ type) appear to be necessary for computation of core-level spectra, both to account for relaxation of the core hole and for convergence of relativistic effects. However, using such bases for all atoms would be quite computationally demanding. The local nature of the core-excitation permits use of a mixed basis strategy⁴³ in which the decontracted triple- ζ basis is only used for the atom whose core-electrons are being

probed, while the corresponding contracted double- ζ basis is sufficient for all other atoms. We have verified that this mixed basis strategy does not lead to any significant change in RMSE of SCAN/SCANh for the species in Tables 1 and 2 (shown in the supporting information) and have employed this strategy for the calculations reported hereon.

In addition, XAS for larger systems is often collected in the solid state or in solution, making it necessary to model the effect of the environment on the calculated spectrum. The locality of core-electrons suggests that only the first coordination shell needs to be considered atomistically for the first few (‘pre edge’) peaks, with a continuum dielectric model being adequate for the remainder of the environment. Such polarizable continuum models (PCM⁹⁸) are likely to be effective for species in which the core electron is excited to a valence level, but would probably be insufficient for Rydberg-like excitations without atomistic modeling of a rather large region around the core-hole. We have employed the integral equation formalism (IEF-) PCM⁹⁹ model to account for environment effects, and thereby investigate how spectra are affected by the phase of the system.¹⁰⁰ IEF-PCM is likely adequate if it only induces a small shift relative to vacuum results, but more sophisticated embedding techniques might prove necessary if there is a significant difference between IEF-PCM and vacuum calculations.

Table 3: Lowest dipole allowed XAS excitation energy for slightly larger species (in eV) from experiment and theory. A mixed basis (aug-pcX-2 on excitation site, aug-pcseg-1 on all other atoms) was utilized for the calculations.

Molecule	Environment	Expt.	SCAN	SCANh
Si (Me) ₄	Gas	1843.6 ¹⁰¹	1843.5	1843.7
Si (OMe) ₄	Gas	1845.9 ¹⁰¹	1845.9	1846.1
(CH ₃ O) ₂ P (S)Cl	Gas	2150.2 ⁹³	2150.0	2150.2
P ₄ O ₆	Gas	2147.5 ¹⁰²	2147.8	2148.0
OP Ph ₃	Solid	2147.3 ²¹	2147.4	2147.7
CF ₃ SF ₅	Gas	2483.8 ¹⁰³	2483.2	2483.6
CH ₃ SS CH ₃	Gas	2471.6 ¹⁰⁴	2472.0	2472.1
(4-Me)C ₆ H ₄ SH	Cyclohexane	2472.5 ⁹	2472.5	2472.7
(4-Me)C ₆ H ₄ S ·	Cyclohexane	2467.0 ⁹	2467.4	2467.5
TiCl ₄	Toluene	2821.6 ¹⁰⁵	2821.3	2821.2

Table 3 shows performance for the mixed basis protocol for molecular systems in the gas phase, or non-polar solvents like cyclohexane (modeled with IEF-PCM, if present). ROKS was used for all closed-shell systems, while single determinant spin-unrestricted Δ SCF was sufficient⁴⁴ for the S 1s \rightarrow SOMO transition of the 4-methylthiophenoxy ((4-Me)C₆H₄S) radical. Our approach appears to be quite accurate in predicting experimental energies, indicating that the OO-DFT/X2C approach can be applied to large molecules for prediction of heavy element K-edges. We also revisited earlier work on light elements,⁴⁴ and demonstrated that inclusion of X2C does not cause any degradation of performance in predicting excitation energies (as shown in the supporting information).

Table 4: Lowest dipole allowed Cl K-edge excitation energy for ionic species (in eV). All experimental data correspond to solid state measurements. ROKS was used for closed-shell species like ClO₄⁻, and spin-unrestricted Δ SCF for open-shell systems like CuCl₄²⁻. A mixed basis set (aug-pcX-2 on excitation site, aug-pcseg-1 on all other atoms) was utilized.

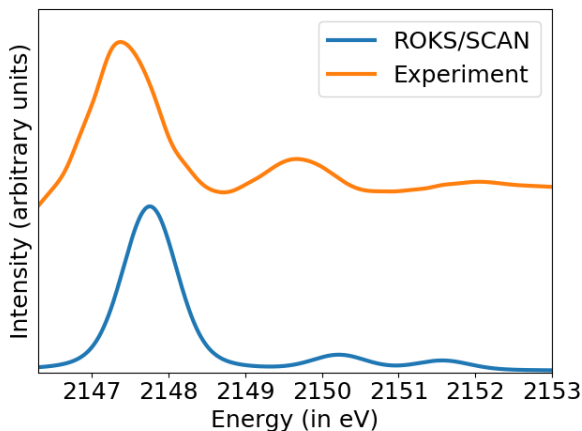
Species	Experiment	Vacuum			Solid		
		SCAN	SCANh	SCAN0	SCAN	SCANh	SCAN0
ClO ₄ ⁻	2835.1 ¹⁰⁶	2834.6	2834.9	2835.4	2834.7	2835.0	2835.4
ClO ₃ ⁻	2831.3 ¹⁰⁶	2830.8	2831.0	2831.4	2830.8	2831.1	2831.4
ClO ₂ ⁻	2826.8 ¹⁰⁶	2826.5	2826.7	2827.0	2826.6	2826.8	2827.1
CuCl ₄ ²⁻	2820.2 ¹⁰⁷	2820.1	2820.3	2820.6	2819.8	2819.9	2820.2
NiCl ₄ ²⁻	2821.5 ¹⁰⁷	2821.4	2821.6	2822.0	2821.1	2821.2	2821.6
CoCl ₄ ²⁻	2822.5 ¹⁰⁷	2822.3	2822.0	2822.5	2821.4	2822.4	2822.1
FeCl ₄ ²⁻	2822.8 ¹⁰⁷	2822.0	2822.3	2822.7	2821.7	2821.9	2822.3
FeCl ₄ ⁻	2820.5 ¹⁰⁷	2820.4	2820.4	2820.4	2820.2	2820.1	2820.1
RMSE		0.4	0.3	0.3	0.6	0.4	0.3
ME		-0.3	-0.2	0.2	-0.6	-0.3	-0.1
MAX		0.8	0.5	0.5	1.1	0.9	0.5

Although we have only considered neutral species so far, core-level spectra of ionic moieties have also been collected in many experiments. These species offer an interesting regime for both testing the efficacy of our approach and for gauging environment effects in general. Table 4 presents a comparison between experiment and theory for Cl K-edges of several ionic species. The ions in Table 4 can be broadly categorized into two categories. The first

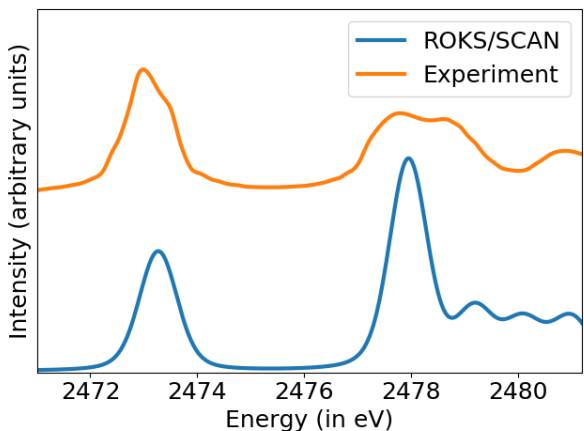
are closed-shell species where Cl has a formally positive oxidation state (ClO_4^- etc) and the lowest excitation is $1s \rightarrow \sigma_{\text{O-Cl}}^*$. These σ^* orbitals are more ‘Cl like’ due to the halogen being electropositive, leading to excitations that are thus mostly localized on the Cl (which is at the center of the ion) and therefore reasonably isolated from the environment. Consequently, not much difference is found between predictions for vacuum, and an IEF-PCM model ionic solid. SCAN, SCANh and SCAN0 all fare reasonably at predicting excitation energies, with the former slightly underestimating and the latter slightly overestimating.

The second class of ions are high-spin tetrahedral transition metal chloride complexes where the lowest transition is charge-transfer (CT) from Cl to a singly occupied metal d level. In addition, the Cl site is on the periphery of the molecule, permitting greater influence from the environment. There is thus a perceptible red-shift in the IEF-PCM results relative to vacuum (due to greater stabilization of the CT like excited state). In addition, SCAN0 appears to be the best performer for this class of excitations. Nonetheless, SCANh appears to do a reasonable job at predicting excitation energies for all of the ionic systems, indicating that the OO-DFT/X2C approach remains capable of delivering semi-quantitative accuracy even outside of small molecules in the gas phase.

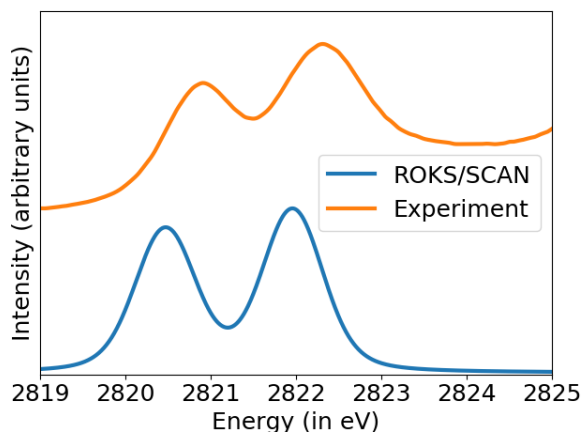
It is also instructive to look beyond computed excitation energies and consider the full spectrum. Fig 4 presents some examples where the experimental spectrum is compared to computed ones, without using any empirical translations. The peak energies align quite well, within the expected error range of ~ 0.5 eV. The peak heights agree less well, although in some cases this is clearly due to the experimental peaks having different widths (such as in Fig 4b for SO_2), vs the uniform broadening utilized for computed spectra. It would be interesting to compute linewidths directly from OO-DFT and determine if that leads to better agreement between theory and experiment. We note that we computed intensities within the dipole-approximation (using transition dipole moments calculated in the manner described in the supporting information and utilizing non-orthogonal configuration interaction techniques¹⁰⁸). It is quite possible that higher order terms have a nonnegligible impact



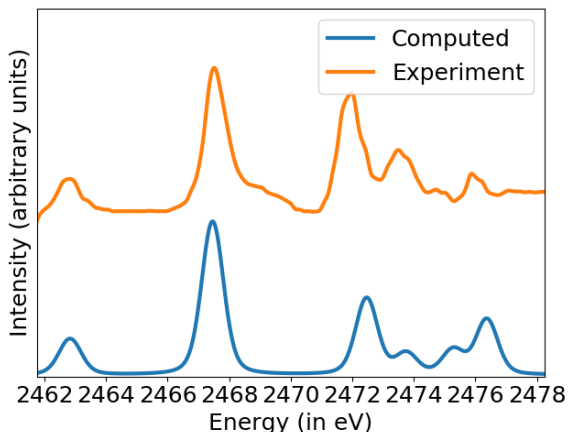
(a) P K-edge XAS of gaseous P_4O_6 ,¹⁰² using a mixed basis (aug-pcX-2 on target P, aug-pcseg-1 on other atoms).



(b) S K-edge XAS of gaseous SO_2 ,⁹⁴ using a doubly augmented (d-aug-) pcX-2 basis on all atoms.



(c) Cl K-edge XAS of solid $[\text{Ph}_4\text{P}]_2\text{TiCl}_6$.²³ The system was approximated with a TiCl_6^{2-} ion, placed in a IEF-PCM dielectric utilizing NaCl parameters ($\epsilon_r = 6, n = 1.5$). A mixed basis (aug-pcX-2 on target Cl, aug-pcseg-1 on other atoms) was used.



(d) Combined S K-edge XAS (> 2470 eV) and S $\text{K}\beta$ emission (< 2470 eV) of gaseous CSO.⁷⁷ ROKS was utilized for the XAS and unrestricted ΔSCF for the emission. A doubly augmented (d-aug-) pcX-2 basis on all atoms was used.

Figure 4: Comparison of experimental K-edge spectra for third period elements, and those computed with SCAN. Computed spectra were broadened with a Voigt profile with a Gaussian standard deviation of 0.3 eV and Lorentzian $\gamma = 0.121$ eV.

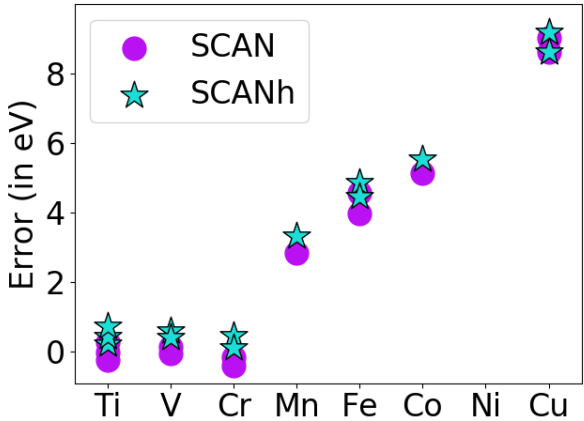
on the experimental X-ray spectrum.¹⁰⁹ Nonetheless, it appears that OO-DFT/X2C is quite effective at reproducing experimental spectra for third period elements.

We next shift our attention to the 3d transition metals. Transition metal complexes are often open-shell, and have several low-lying orbitals that core electrons can be excited to.

Table 5: Lowest symmetry allowed transition metal K-edge transitions. Δ SCF was used for $1s \rightarrow$ SOMO transitions of open-shell systems like $\text{VO}(\text{acac})_2$, while ROKS was used for closed-shell species like TiCl_4 . A mixed basis (decontracted aug-cc-p ω CVTZ¹¹⁶ on excitation site, aug-cc-pVDZ on all other atoms) was utilized. Experimental data corresponds to the solid state for all species other than TiCl_4 , whose spectrum was collected in toluene solution.

	Experiment	SCAN	SCANh
TiCl_4	4969.2 ¹⁰⁵	4968.9	4969.4
TiCpCl_3	4968.1 ¹⁰⁵	4968.1	4968.5
TiCp_2Cl_2	4967.3 ¹⁰⁵	4967.5	4968.0
$\text{VO}(\text{acac})_2$	5468.4 ¹¹⁰	5468.6	5469.0
VCp_2Cl_2	5468.4 ¹¹⁰	5468.3	5468.8
CrO_4^{2-}	5996.5 ¹¹¹	5996.3	5996.9
$\text{Cr}_2\text{O}_7^{2-}$	5996.6 ¹¹¹	5996.2	5996.7
MnO_4^-	6543.3 ¹¹²	6546.1	6546.6
FeCp_2	7111.9 ¹¹³	7116.5	7116.8
FeCl_4^-	7113.2 ³	7117.1	7117.6
CoCl_4^{2-}	7709.2 ¹¹⁴	7714.3	7714.7
CuCl_4^{2-}	8977.6 ¹¹⁵	8986.6	8986.8
$\text{Cu}(\text{CF}_3)_4^-$	8981.8 ¹¹⁵	8990.4	8990.4

(a) Individual values (in eV)



(b) Excitation energy error vs nuclear charge.

K-edge spectra of these species are therefore widely studied, despite the $1s \rightarrow 3d$ transition in bare atoms being dipole forbidden. Indeed, the transition in centrosymmetric entities (like octahedral complexes) can only be driven by electric quadrupole terms or vibrational symmetry breaking.^{3,117} Tetrahedral complexes however can have some p-d mixing, leading to some dipole allowed intensity for K-edge transitions.¹¹⁷ Furthermore, X-ray emission spectra (XES) can be collected for $2p/3p \rightarrow 1s$ excitations, yielding further useful information.²

Table 5 shows the performance of OO-DFT in predicting transition metal K-edge energies, with the SCAN and SCANh functionals. The results are quite adequate for Ti, V, and Cr but performance is significantly degraded for heavier transition metals like Mn, Fe, Co and Cu due to significant overestimation (as made evident by Table 5b). This is quite interesting, as SCAN had a slight penchant for underestimation when it came to lighter elements, unlike the significant overbinding observed here for Cu, Co and Fe (beyond the scale of typical OO-DFT errors). It should be noted that many of the species in Table 5 are high-spin tetrahedral

complexes like FeCl_4^- , CoCl_4^{2-} and CuCl_4^{2-} or d^0 species like TiCl_4 , CrO_4^{2-} and MnO_4^- . These species are therefore not particularly multireference, removing one possible source of the error.

The steep increase in the error with increasing Z appears to suggest a relativistic origin. Indeed, the spin-free one-electron X2C model employed in our work is hardly complete, as it does not include vector (spin-orbit) terms, finite nucleus size effects, or any relativistic contributions to the two-electron terms. The spin-orbit terms are unlikely to be relevant for K-edges, and the finite nucleus size effects are quite small for such elements (being only 0.3 eV for Kr¹¹⁸ and therefore smaller for lighter elements). The missing two-electron pieces however are of a comparable magnitude to the error. Specifically, X2C does not transform the electron-electron repulsion terms (the so-called “picture-change”⁶¹), incorporate additional (Breit)¹¹⁹ contributions to the electron-electron interaction, or account for quantum electrodynamic effects. These additional terms were previously found to sum to ~ 20 eV of underbinding for the Kr K-edge,^{68,118,120} indicating that overestimation by a few eVs is quite possible for heavier fourth period elements from lack of such effects alone.

We attempted to estimate of the magnitude of missing effects via four-component Dirac-HF (DHF) calculations to account for the picture change and Breit terms, and a QED correction via extrapolation from data in Ref. 120. Specifically, we obtain a Koopmans-level estimate¹²¹ for the first two quantities via computing the difference between the spin-free one-electron X2C 1s eigenvalue and the corresponding DHF eigenvalue for 3d transition metal atomic cations (listed in the supporting information). This analysis reveals that the spin-free X2C one-electron Hamiltonian overbinds by 10.3 eV for Cu^{2+} , which is comparable to the errors seen in Table 5. However, these contributions amount to 3.9 eV for Ti^{4+} , indicating that they are very much relevant even for lighter elements (including the third period elements Si–Cl¹²²). It therefore appears that the good performance of OO-DFT/X2C in this regime is partly due to cancellation of errors between the missing relativistic contributions and the functional error from SCAN. The sudden increase in error on going from Cr to Mn

therefore appears to stem from a breakdown of the error cancellation. The somewhat dramatic increase in error is surprising, but experimental uncertainties in this regime are usually ~ 1 eV and Z is a discrete, integer-valued variable, making such sudden increases possible. It should also be noted that the missing relativistic corrections discussed here are estimated at a Koopmans’ theorem based level and so can differ somewhat from a full OO-DFT estimate (which we cannot find at present).

However, it is worth stressing that the X2C model nonetheless manages to account for the vast majority of relativistic effects for even species like Cu/Kr. It is also worth noting that translating OO-DFT/X2C metal K-edge spectra for alignment with experiment would involve much smaller shifts than TDDFT, reducing the magnitude of potential translation driven error. Nonetheless, we wish to avoid any need for empirical translation of spectra, and instead intend to pursue more accurate relativistic models to quantitatively model the K-edge spectra of heavier elements.

Table 6: Lowest symmetry allowed L-edge (2p) transitions for transition metal containing species (in eV). Δ SCF was used for 2p \rightarrow SOMO transitions of open-shell systems like CuCl_4^{2-} , while ROKS was used for closed-shell species like ferrocene (FeCp_2). Computed multiplet averaged energies (found from averaging over all the 2p orbitals) were red-shifted by J (where $3J$ is the experimental energy gap between the L_2 and L_3 peaks) to better approximate the experimental L_3 peaks. A mixed basis (decontracted aug-cc-p ω CVTZ on excitation site, aug-cc-pVDZ on all other atoms) was utilized for the calculations.

	Experiment			Theoretical L_3 edge		
	L_3	L_2	$3J=L_2-L_3$	SCAN	SCANh	SCAN0
TiCl_4	456.9 ¹²³	462.5	5.6	455.9	456.4	457.1
$\text{Mn}(\text{OH}_2)_6^{2+}$	639.7 ¹²⁴	649.1	9.4	638.7	638.9	639.3
$\text{Fe}(\text{CN})_6^{3-}$	705.8 ¹²⁵	718.4	12.6	706.1	706.5	707.1
FeCp_2	708.9 ¹²⁶	721.2	12.3	708.2	708.5	709.0
CuCl_4^{2-} (D_{2h})	930.1 ¹¹⁵	950.1	20	929.4	929.5	929.8
$\text{Cu}(\text{CF}_3)_4^-$	934.7 ¹¹⁵	954.7	20	933.5	933.5	933.7

Metal L-edge (2p) spectra are also extensively studied via experiment. Accurate computation of spectra necessitates going beyond the scalar relativistic paradigm as the degeneracy of the 2p levels is broken by spin-orbit coupling. Scalar relativistic models like X2C

can potentially yield a reasonable estimate for the multiplet averaged peak, which can be subsequently shifted by atomic spin-orbit values to obtain the experimentally observed $L_{3/2}$ (L_3 -edge) and $L_{1/2}$ (L_2 -edge) multiplet peaks. This strategy has been found to be effective for L-edges of Si,P,S and Cl.⁴³ However, it is less appealing for heavier elements due to the larger magnitude of the multiplet splitting (20 eV for Cu vs 1.6 eV for Cl), which can potentially exert a direct influence in the OO process. We have nonetheless applied this measure to compute L-edges for a few 3d metal containing species (shown in Table 6), to assess this approach. It is quite apparent that the errors are much larger here (relative to Fig 3), with significant underestimation being the norm for all species aside for $[\text{Fe}(\text{CN})_6]^{3+}$. The results are also often quite sensitive to % HF exchange (more so than most of the species considered till this point). Nonetheless, the worst case errors are just slightly above 1 eV, indicating that OO-DFT with proper inclusion of spin-orbit effects and careful functional choice has the potential to be quite accurate in predicting metal L-edges. We are presently investigating this aspect further.

Overall, it is clear that the OO-DFT/X2C combination is capable of consistently delivering < 1 eV error for core-level excitation/ionization energies for third period elements and reproduce experimental spectra fairly well. Indeed, the typical error is ~ 0.5 eV for SCAN/SCANh, as shown by Fig 3 and the RMSEs reported in Tables 1 and 2. X2C therefore extends the applicability of OO-DFT methods to elements heavier than F, which was previously the limit for computational core-level spectroscopy with such methods (without post-facto application of ad-hoc relativistic corrections). OO-DFT X2C also appears to be adequate for the K-edges of the transition metals Ti, V and Cr. However, performance degrades starting with Mn, possibly due to lack of relativistic effects in the two-electron interaction terms. The spin-free X2C model is also incapable of accounting for the spin-orbit splitting observed in experimental L-edge spectra. Accounting for these effects would be critical for extension of OO-DFT beyond the cases explored in this work. We are also attempting to apply OO-DFT extensively to K-edge spectra of third period elements, in order

to uncover any additional limitations of the approach. Any resulting insight could also prove valuable in training density functionals that are accurate in modeling both ground states and OO-DFT excited states, as it is quite possible that not much further improvement in prediction quality can be obtained from functionals trained solely for the ground state.

Computational methods

All calculations were performed with a development version of the Q-Chem 5.4 package¹²⁷ and these new capabilities will be publicly available with the next release of code. Local exchange–correlation integrals for DFT were calculated over a radial grid with 99 points and an angular Lebedev grid with 590 points. Ref 44 lays out the protocol for computing Δ SCF excited states, while Ref 43 does the same for ROKS. The restricted open-shell optimizations necessary in this process were performed through square gradient minimization (SGM³⁹) and unrestricted optimizations with initial maximum overlap method (IMOM³⁶). The core-hole was localized onto a single atom for species with equivalent atoms (like S in CS₂), in order to prevent errors arising from delocalization^{128,129} of the hole over multiple sites.⁴³ Standard values of dielectric constant ϵ_r and refractive index n were used for IEF-PCM modeling of common solvents like cyclohexane (listed in the supporting information). The corresponding data for most solid state materials was not available, and consequently all solid state environments were modeled with NaCl parameters ($\epsilon_r = 6, n = 1.5$). This should be reasonable for ionic solids, although perhaps a little too polar for molecular solids like OPPh₃ (Table 3). However, the resulting values for OPPh₃ were quite close to vacuum calculations (as shown in the supporting information), suggesting that the environment exerted negligible impact on the spectrum. Four-component DHF calculations for 3d transition metal ions were carried out within the PySCF package.¹³⁰

Experimental geometries were used whenever possible, through gas phase data from NIST¹³¹ or crystal structures from the Cambridge structural database.¹³² Structures were

optimized with ω B97M-V¹³³/aug-pcseg-1 under gas phase conditions, if experimental data was unavailable. The source of all of the geometries is listed in the supporting information, along with the associated atomic coordinates. In particular, the CuCl_4^{2-} ion studied is of D_{2h} (distorted tetrahedral) symmetry, corresponding to Cs_2CuCl_4 .¹³⁴ The ground state geometries were employed for excited state calculations, consistent with the Franck-Condon principle.^{135,136}

Acknowledgment

This work was supported by the Liquid Sunlight Alliance, which is funded by the U.S. Department of Energy, Office of Science, Office of Basic Energy Sciences, Fuels from Sunlight Hub under Award Number DE-SC0021266 with additional support from the Director, Office of Science, Office of Basic Energy Sciences, of the U.S. Department of Energy, under Contract No. DE-AC02-05CH11231. We would like to thank Prof. Lan Cheng for helpful discussions.

Supporting Information

PDF: X2C transformation, validation, short note about S K-edge binding energies of some species, short note on computing transition dipole moments.

XLXS: Basis set convergence, light element data, functional screening information, X2C validation, post spin-free X2C one electron relativistic contributions.

ZIP: Geometries of all species considered in xyz format (along with provenance).

Conflicts of Interest

M.H.-G. is a part-owner of Q-Chem, which is the software platform in which the developments described here were implemented.

Supporting Information

Exact Two-Component (X2C) Relativistic Hamiltonian

The starting point for deriving the X2C relativistic model is the four-component one-electron Dirac Hamiltonian (Eq 1) represented in a restricted kinetic balance (RKB) form.¹³⁷ Our goal is to use a unitary transformation that effectively decouples the positive and negative-energy solutions of the Dirac equation, since we are only interested in describing electrons. In Eq. 1, T , V and S are the usual non-relativistic kinetic energy, nuclear attraction and overlap matrices, respectively, represented in a basis of atomic orbitals $\{\phi_\mu\}$. W is defined as the matrix representation of the operator in Eq. 2, where $\vec{\sigma}$ is the vector of Pauli matrices, and \vec{p} and V are the momentum and nuclear-attraction operators, respectively. As indicated in Eq 2, \hat{W} can be decomposed into spin-free (\hat{W}_{SF}) and spin-orbit (\hat{W}_{SO}) components (likewise, the matrix representation W can also be separated into W_{SF} and W_{SO}). Finally, the solutions of Eq. 1 are characterized by their large (C_L) and small (C_S) components.

$$\begin{bmatrix} V & T \\ T & \frac{W}{4c^2} - T \end{bmatrix} \begin{bmatrix} C_L \\ C_S \end{bmatrix} = E \begin{bmatrix} S & 0 \\ 0 & \frac{1}{2c^2}T \end{bmatrix} \begin{bmatrix} C_L \\ C_S \end{bmatrix} \quad (1)$$

$$\hat{W} = (\vec{\sigma} \cdot \vec{p})V(\vec{\sigma} \cdot \vec{p}) = (\vec{p} \cdot V\vec{p} + i\vec{\sigma} \cdot (\vec{p} \times V\vec{p})) = \hat{W}_{\text{SF}} + i\vec{\sigma} \cdot \hat{W}_{\text{SO}} \quad (2)$$

$$W_{\mu\nu} = \langle \phi_\mu | \hat{W} | \phi_\nu \rangle \quad (3)$$

As outlined in the main text, we focused on the inclusion of scalar relativistic effects to OO-DFT, so only the spin-free W_{SF} was taken into account and the spin-orbit W_{SO} ignored. It is possible to evaluate the matrix elements of W_{SF} analytically in a gaussian type orbital (GTO) basis, but we chose to take a finite difference approach instead, which can be readily utilized by any quantum chemistry code without too much difficulty.

Our approach is based on the momentum operator being a generator of translation. We

know that given a basis function $\phi_\mu(\vec{r})$ (GTO or otherwise), we have:

$$\phi_\mu(\vec{r} + \delta\hat{n}) = T(\delta\hat{n})\phi_\mu(\vec{r}) \quad (4)$$

where the translation operator $T(\delta\hat{n}) = \exp(-i\delta\hat{n} \cdot \vec{p})$ translates the orbital by δ along the unit vector \hat{n} . With this, we can see that:

$$(\hat{n} \cdot \vec{p}) \phi_\mu(\vec{r}) = -i \frac{\phi_\mu(\vec{r} + \delta\hat{n}) - \phi_\mu(\vec{r} - \delta\hat{n})}{2\delta} + O(\delta^2) \quad (5)$$

which can also be obtained from noting that the momentum operator $(\hat{n} \cdot \vec{p})$ along \hat{n} is equivalent to taking the derivative with respect to the spatial coordinate along \hat{n} . We can thus define a finite difference momentum operator $\vec{p}_2(\delta)$ such that:

$$(\hat{x} \cdot \vec{p}_2(\delta)) \phi_\mu(\vec{r}) = -i \frac{\phi_\mu(\vec{r} + \delta\hat{x}) - \phi_\mu(\vec{r} - \delta\hat{x})}{2\delta} \quad (6)$$

$$(\hat{y} \cdot \vec{p}_2(\delta)) \phi_\mu(\vec{r}) = -i \frac{\phi_\mu(\vec{r} + \delta\hat{y}) - \phi_\mu(\vec{r} - \delta\hat{y})}{2\delta} \quad (7)$$

$$(\hat{z} \cdot \vec{p}_2(\delta)) \phi_\mu(\vec{r}) = -i \frac{\phi_\mu(\vec{r} + \delta\hat{z}) - \phi_\mu(\vec{r} - \delta\hat{z})}{2\delta} \quad (8)$$

Consequently, an approximate $\hat{W}_{2,\text{SF}}$ can be defined as:

$$\hat{W}_{2,\text{SF}}(\delta) = \vec{p}_2(\delta) \cdot V \vec{p}_2(\delta) \quad (9)$$

$$= (\hat{x} \cdot \vec{p}_2(\delta)) V (\hat{x} \cdot \vec{p}_2(\delta)) + (\hat{y} \cdot \vec{p}_2(\delta)) V (\hat{y} \cdot \vec{p}_2(\delta)) + (\hat{z} \cdot \vec{p}_2(\delta)) V (\hat{z} \cdot \vec{p}_2(\delta)) \quad (10)$$

The resulting matrix elements can be found in the following manner:

$$\begin{aligned} & \phi_\mu^*(\vec{r}) (\hat{x} \cdot \vec{p}_2(\delta)) V (\hat{x} \cdot \vec{p}_2(\delta)) \phi_\nu(\vec{r}) \\ &= (\hat{x} \cdot \vec{p}_2(\delta) \phi_\mu(\vec{r}))^* V (\hat{x} \cdot \vec{p}_2(\delta) \phi_\nu(\vec{r})) \end{aligned} \quad (11)$$

$$\begin{aligned} &= \frac{1}{4\delta^2} (\phi_\mu(\vec{r} + \delta\hat{x})V\phi_\nu(\vec{r} + \delta\hat{x}) + \phi_\mu(\vec{r} - \delta\hat{x})V\phi_\nu(\vec{r} - \delta\hat{x}) \\ &\quad - \phi_\mu(\vec{r} - \delta\hat{x})V\phi_\nu(\vec{r} + \delta\hat{x}) - \phi_\mu(\vec{r} + \delta\hat{x})V\phi_\nu(\vec{r} - \delta\hat{x})) \end{aligned} \quad (12)$$

Thus matrix elements of $W_{2,\text{SF}}$ can be found via evaluation of matrix elements of V using slightly translated GTOs $\phi_\mu(\vec{r} + \delta\hat{x})$ etc, which should be not too challenging for any quantum chemistry code. The resulting values will however have some finite difference error as:

$$W_{\text{SF}} = W_{2,\text{SF}}(\delta) + O(\delta^2) \quad (13)$$

This error can be greatly reduced by utilizing different values of δ and refining W_{SF} via:

$$W_{\text{SF}} = \frac{W_{2,\text{SF}}(2\delta) - 16W_{2,\text{SF}}(\delta) + 64W_{2,\text{SF}}\left(\frac{\delta}{2}\right)}{45} + O(\delta^6) \quad (14)$$

or other higher order stencils. We used Eq 14 in our implementation with $\delta = 1 \times 10^{-4}$ atomic units, resulting in negligible finite difference error.

One can obtain the coupling matrix X for the positive energy solutions of Eq. 1 as the ratio between the large and small components, as indicated in Eq. 15. The renormalization matrix R is then defined as in Eq. 16, where \tilde{S} (Eq. 17) is a modified overlap matrix that takes into account the folding of the small component into the large one.

$$X = C_S(C_L)^{-1} \quad (15)$$

$$R = S^{-1/2} \left(S^{-1/2} \tilde{S} S^{-1/2} \right)^{-1/2} S^{1/2} \quad (16)$$

$$\tilde{S} = S + X^\dagger \frac{1}{2c^2} X \quad (17)$$

With the X and R matrices, we can now calculate the effective SF-X2C1e kinetic energy (Eq. 18) and nuclear attraction (Eq. 19) operators for subsequent KS-DFT calculations.

$$T_{X2C} = R^\dagger (TX + X^\dagger T - X^\dagger TX) R \quad (18)$$

$$V_{X2C} = R^\dagger \left(V + \frac{1}{4c^2} X^\dagger W_{SF} X \right) R \quad (19)$$

We checked our finite differences implementation with the analytical one from the Psi4 package¹³⁸ by comparing absolute Hartree-Fock (HF) energies. Table 7 indicates that the energy difference between the two implementations is usually on the order of 10^{-7} hartrees or less (which should have negligible impact on core-level spectrum calculations).

Table 7: Absolute ground state HF energies obtained with Psi4’s analytical implementation of X2C and Q-Chem’s finite differences. A comparison of non-relativistic energies is also supplied for comparison. The decontracted aug-cc-pCVTZ basis was used for SiH₄,PH₃,HCl and Ar; while decontracted cc-pVDZ was used for the transition metal containing systems.

System	Non-relativistic ground state total energy			X2C ground state total energy		
	Psi4	Q-Chem	Difference	Psi4	Q-Chem	Difference
SiH ₄	-291.2641256030	-291.2641256030	-2.0E-11	-291.8673077884	-291.8673077905	-2.1E-09
PH ₃	-342.4903826664	-342.4903826663	7.0E-11	-343.3071475141	-343.3071475130	1.1E-09
H ₂ S	-398.7160009253	-398.7160009254	-7.0E-11	-399.7996418715	-399.7996419031	-3.2E-08
HCl	-460.1087555150	-460.1087555151	-1.5E-10	-461.5217242958	-461.5217242810	1.5E-08
Ar	-526.8134620705	-526.8134620705	2.0E-11	-528.6278041021	-528.6278041049	-2.8E-09
TiCl ₄	-2686.7122452582	-2686.7122452457	1.3E-08	-2696.7140080590	-2696.7140080397	1.9E-08
CrO ₄ ²⁻	-1342.4736099183	-1342.4736099171	1.2E-09	-1349.0259066545	-1349.0259066508	3.7E-09
MnO ₄ ⁻	-1448.7946004947	-1448.7946004920	2.7E-09	-1456.5639058910	-1456.5639058892	1.8E-09
FeCl ₄ ²⁻	-3100.7604247005	-3100.7604246828	1.8E-08	-3115.3237860409	-3115.3237860275	1.3E-08
CoCl ₄ ²⁻	-3219.7195689779	-3219.7195689046	7.3E-08	-3235.8506032331	-3235.8506031501	8.3E-08
NiCl ₄ ²⁻	-3345.1648205253	-3345.1648204645	6.1E-08	-3363.0642419690	-3363.0642419050	6.4E-08
CuCl ₄ ²⁻	-3477.2188051504	-3477.2188050680	8.2E-08	-3497.1060177623	-3497.1060176503	1.1E-07

Note on binding energies for some S compounds

The 1s binding energies for several S compounds in Table 1 of the main paper were obtained from Ref 78, which reported how much those energies differed from the 1s ionization energy of H₂S. However, the reference energy for H₂S reported by Ref 78 was in error by 0.5 eV, as a relativistic effect was missed during calibration of experiment.^{139,140} We therefore used the H₂S 1s binding energy from Ref 76 (which was validated by subsequent studies^{139,140}) as the reference, and added the shifts reported by Ref 78 to obtain the true binding energies. This protocol should be acceptable, as the shifts reported in Ref 78 should not be affected by the error in the reference value.^{139,140}

Note on computing transition dipole moments

The transition dipole moments for excitations described in this work were computed by treating the KS Slater determinants as pseudo-wavefunctions. In other words, if the ground state of a species has a KS determinant $|\Phi_0\rangle$ and the Δ SCF excited state has a KS determinant $|\Phi_n\rangle$, the transition dipole moment between them is given by:

$$\vec{\mu}_{0n} = \langle \Phi_0 | \hat{\mu} | \Phi_n \rangle \quad (20)$$

where $\hat{\mu}$ is the dipole operator.

For ROKS, there are two excited state determinants with equal weight (corresponding to the exchange of up and down spins). If those determinants are $|\Phi_n\rangle$ and $|\bar{\Phi}_n\rangle$ respectively, the ROKS ‘wave function’ is $\frac{|\Phi_n\rangle + |\bar{\Phi}_n\rangle}{\sqrt{2}}$, leading to a transition dipole of:

$$\vec{\mu}_{0n} = \frac{1}{\sqrt{2}} \left(\langle \Phi_0 | \hat{\mu} | \Phi_n \rangle + \langle \Phi_0 | \hat{\mu} | \bar{\Phi}_n \rangle \right) \quad (21)$$

$$= \sqrt{2} \langle \Phi_0 | \hat{\mu} | \Phi_n \rangle \quad (22)$$

if the ground state $|\Phi_0\rangle$ is closed-shell (from spin-inversion symmetry, as $\hat{\mu}$ is purely a spatial one-particle operator).

Computation of $\langle \Phi_0 | \hat{\mu} | \Phi_n \rangle$ is not quite straightforward as the two determinants are constructed from different (non-orthogonal) sets of orbitals. Non-orthogonal configuration interaction techniques (as described in Ref 108) have to be therefore employed, incurring some extra computational cost vs cases with orthogonal orbitals, but ultimately having negligible effect relative to the cost of excited state orbital optimization.

One further point to note is that $\vec{\mu}_{0n}$ is not translationally invariant for cases with $\langle \Phi_0 | \Phi_n \rangle \neq 0$. This is easily resolved in neutral systems via inclusion of the nuclear contribution to the $\hat{\mu}$ operator, which restores translational invariance (and which amounts to translating the system to the center of nuclear charge). For charged systems, it is necessary

to directly translate the system to the center of nuclear charge in order to have results that are not heavily contaminated by spurious contributions from the nonzero overlap $\langle \Phi_0 | \Phi_n \rangle$. Alternatively, symmetric orthogonalization¹⁴¹ can be carried out to obtain translationally invariant results. Both routes give similar results for valence Δ SCF on neutral systems¹⁴¹ and we have therefore used the simpler route of operating from the center of nuclear charge for the small systems examined in Fig 4 of the main manuscript.

References

- (1) Yuhas, B. D.; Fakra, S.; Marcus, M. A.; Yang, P. Probing the local coordination environment for transition metal dopants in zinc oxide nanowires. *Nano Lett.* **2007**, *7*, 905–909.
- (2) Pollock, C. J.; DeBeer, S. Insights into the geometric and electronic structure of transition metal centers from valence-to-core X-ray emission spectroscopy. *Acc. Chem. Res.* **2015**, *48*, 2967–2975.
- (3) Westre, T. E.; Kennepohl, P.; DeWitt, J. G.; Hedman, B.; Hodgson, K. O.; Solomon, E. I. A multiplet analysis of Fe K-edge $1s \rightarrow 3d$ pre-edge features of iron complexes. *J. Am. Chem. Soc.* **1997**, *119*, 6297–6314.
- (4) Solomon, E. I.; Hedman, B.; Hodgson, K. O.; Dey, A.; Szilagy, R. K. Ligand K-edge X-ray absorption spectroscopy: covalency of ligand–metal bonds. *Coord. Chem. Rev.* **2005**, *249*, 97–129.
- (5) Kubin, M.; Guo, M.; Kroll, T.; Löchel, H.; Källman, E.; Baker, M. L.; Mitzner, R.; Gul, S.; Kern, J.; Föhlisch, A. et al. Probing the oxidation state of transition metal complexes: a case study on how charge and spin densities determine Mn L-edge X-ray absorption energies. *Chem. Sci.* **2018**, *9*, 6813–6829.
- (6) Chergui, M.; Collet, E. Photoinduced structural dynamics of molecular systems mapped by time-resolved X-ray methods. *Chem. Rev.* **2017**, *117*, 11025–11065.
- (7) Bhattacharjee, A.; Leone, S. R. Ultrafast X-ray Transient Absorption Spectroscopy of Gas-Phase Photochemical Reactions: A New Universal Probe of Photoinduced Molecular Dynamics. *Acc. Chem. Res.* **2018**, *51*, 3203–3211.
- (8) Kraus, P. M.; Zürich, M.; Cushing, S. K.; Neumark, D. M.; Leone, S. R. The ultrafast X-ray spectroscopic revolution in chemical dynamics. *Nat. Rev. Chem.* **2018**, *2*, 82–94.

- (9) Ochmann, M.; Von Ahnen, I.; Cordones, A. A.; Hussain, A.; Lee, J. H.; Hong, K.; Adamczyk, K.; Vendrell, O.; Kim, T. K.; Schoenlein, R. W. et al. Light-induced radical formation and isomerization of an aromatic thiol in solution followed by time-resolved x-ray absorption spectroscopy at the sulfur K-edge. *J. Am. Chem. Soc.* **2017**, *139*, 4797–4804.
- (10) Bhattacharjee, A.; Pemmaraju, C. D.; Schnorr, K.; Attar, A. R.; Leone, S. R. Ultrafast intersystem crossing in acetylacetone via femtosecond x-ray transient absorption at the carbon K-edge. *J. Am. Chem. Soc.* **2017**, *139*, 16576–16583.
- (11) Dreuw, A.; Head-Gordon, M. Single-reference ab initio methods for the calculation of excited states of large molecules. *Chem. Rev.* **2005**, *105*, 4009–4037.
- (12) Krylov, A. I. Equation-of-motion coupled-cluster methods for open-shell and electronically excited species: The hitchhiker’s guide to Fock space. *Annu. Rev. Phys. Chem.* **2008**, *59*, 433–462.
- (13) Runge, E.; Gross, E. K. U. Density-functional theory for time-dependent systems. *Phys. Rev. Lett.* **1984**, *52*, 997–1000.
- (14) Wenzel, J.; Wormit, M.; Dreuw, A. Calculating core-level excitations and x-ray absorption spectra of medium-sized closed-shell molecules with the algebraic-diagrammatic construction scheme for the polarization propagator. *J. Comput. Chem.* **2014**, *35*, 1900–1915.
- (15) Lopata, K.; Van Kuiken, B. E.; Khalil, M.; Govind, N. Linear-response and real-time time-dependent density functional theory studies of core-level near-edge x-ray absorption. *J. Chem. Theo. Comput.* **2012**, *8*, 3284–3292.
- (16) Besley, N. A. Modeling of the spectroscopy of core electrons with density functional theory. *WIREs Comput. Mol. Sci.* **2021**, e1527.

- (17) Zhang, Y.; Biggs, J. D.; Healion, D.; Govind, N.; Mukamel, S. Core and valence excitations in resonant X-ray spectroscopy using restricted excitation window time-dependent density functional theory. *J. Chem. Phys.* **2012**, *137*, 194306.
- (18) Besley, N. A. Density functional theory based methods for the calculation of X-ray spectroscopy. *Acc. Chem. Res.* **2020**, *53*, 1306–1315.
- (19) Besley, N. A.; Peach, M. J.; Tozer, D. J. Time-dependent density functional theory calculations of near-edge X-ray absorption fine structure with short-range corrected functionals. *Phys. Chem. Chem. Phys.* **2009**, *11*, 10350–10358.
- (20) Besley, N. A.; Asmuruf, F. A. Time-dependent density functional theory calculations of the spectroscopy of core electrons. *Phys. Chem. Chem. Phys.* **2010**, *12*, 12024–12039.
- (21) Blake, A. V.; Wei, H.; Donahue, C. M.; Lee, K.; Keith, J. M.; Daly, S. R. Solid energy calibration standards for P K-edge XANES: electronic structure analysis of PPh₄Br. *J. Synchrotron Radiat.* **2018**, *25*, 529–536.
- (22) Martin-Diaconescu, V.; Kennepohl, P. Sulfur K-edge XAS as a probe of sulfur-centered radical intermediates. *J. Am. Chem. Soc.* **2007**, *129*, 3034–3035.
- (23) Minasian, S. G.; Keith, J. M.; Batista, E. R.; Boland, K. S.; Clark, D. L.; Conradson, S. D.; Kozimor, S. A.; Martin, R. L.; Schwarz, D. E.; Shuh, D. K. et al. Determining relative f and d orbital contributions to M–Cl covalency in MCl₆²⁻ (M= Ti, Zr, Hf, U) and UOCl₅⁻ using Cl K-edge X-ray absorption spectroscopy and time-dependent density functional theory. *J. Am. Chem. Soc.* **2012**, *134*, 5586–5597.
- (24) DeBeer George, S.; Petrenko, T.; Neese, F. Prediction of iron K-edge absorption spectra using time-dependent density functional theory. *J. Phys. Chem. A* **2008**, *112*, 12936–12943.

- (25) Attar, A. R.; Bhattacharjee, A.; Pemmaraju, C.; Schnorr, K.; Closser, K. D.; Prendergast, D.; Leone, S. R. Femtosecond x-ray spectroscopy of an electrocyclic ring-opening reaction. *Science* **2017**, *356*, 54–59.
- (26) Stanton, J. F.; Bartlett, R. J. The equation of motion coupled-cluster method. A systematic biorthogonal approach to molecular excitation energies, transition probabilities, and excited state properties. *J. Chem. Phys.* **1993**, *98*, 7029–7039.
- (27) Coriani, S.; Koch, H. Communication: X-ray absorption spectra and core-ionization potentials within a core-valence separated coupled cluster framework. *J. Chem. Phys.* **2015**, *143*, 181103.
- (28) Peng, B.; LeStrange, P. J.; Goings, J. J.; Caricato, M.; Li, X. Energy-specific equation-of-motion coupled-cluster methods for high-energy excited states: Application to K-edge X-ray absorption spectroscopy. *J. Chem. Theo. Comput.* **2015**, *11*, 4146–4153.
- (29) Frati, F.; De Groot, F.; Cerezo, J.; Santoro, F.; Cheng, L.; Faber, R.; Coriani, S. Coupled cluster study of the x-ray absorption spectra of formaldehyde derivatives at the oxygen, carbon, and fluorine K-edges. *J. Chem. Phys.* **2019**, *151*, 064107.
- (30) Vidal, M. L.; Feng, X.; Epifanovsky, E.; Krylov, A. I.; Coriani, S. New and efficient equation-of-motion coupled-cluster framework for core-excited and core-ionized states. *J. Chem. Theory Comput.* **2019**, *15*, 3117–3133.
- (31) Carbone, J. P.; Cheng, L.; Myhre, R. H.; Matthews, D.; Koch, H.; Coriani, S. An analysis of the performance of coupled cluster methods for K-edge core excitations and ionizations using standard basis sets. *Adv. Quantum Chem.* **2019**, *79*, 241–261.
- (32) Besley, N. A.; Gilbert, A. T.; Gill, P. M. W. Self-consistent-field calculations of core excited states. *J. Chem. Phys.* **2009**, *130*, 124308.

- (33) Hait, D.; Head-Gordon, M. Orbital optimized density functional theory for electronic excited states. *J. Phys. Chem. Lett.* **2021**, *12*, 4517–4529.
- (34) Derricotte, W. D.; Evangelista, F. A. Simulation of X-ray absorption spectra with orthogonality constrained density functional theory. *Phys. Chem. Chem. Phys.* **2015**, *17*, 14360–14374.
- (35) Zheng, X.; Liu, J.; Doumy, G.; Young, L.; Cheng, L. Hetero-site Double Core Ionization Energies with Sub-electronvolt Accuracy from Delta-Coupled-Cluster Calculations. *J. Phys. Chem. A* **2020**, *124*, 4413–4426.
- (36) Barca, G. M.; Gilbert, A. T.; Gill, P. M. W. Simple Models for Difficult Electronic Excitations. *J. Chem. Theory Comput.* **2018**, *14*, 1501–1509.
- (37) Shea, J. A.; Gwin, E.; Neuscammann, E. A generalized variational principle with applications to excited state mean field theory. *J. Chem. Theory Comput.* **2020**, *16*, 1526–1540.
- (38) Ye, H.-Z.; Welborn, M.; Ricke, N. D.; Van Voorhis, T. σ -SCF: A direct energy-targeting method to mean-field excited states. *J. Chem. Phys.* **2017**, *147*, 214104.
- (39) Hait, D.; Head-Gordon, M. Excited state orbital optimization via minimizing the square of the gradient: General approach and application to singly and doubly excited states via density functional theory. *J. Chem. Theory Comput.* **2020**, *16*, 1699–1710.
- (40) Carter-Fenk, K.; Herbert, J. M. State-Targeted Energy Projection: A Simple and Robust Approach to Orbital Relaxation of Non-Aufbau Self-Consistent Field Solutions. *J. Chem. Theory Comput.* **2020**, *16*, 5067–5082.
- (41) Levi, G.; Ivanov, A. V.; Jónsson, H. Variational density functional calculations of excited states via direct optimization. *J. Chem. Theory Comput.* **2020**, *16*, 6968–6982.

- (42) Grofe, A.; Zhao, R.; Wildman, A.; Stetina, T. F.; Li, X.; Bao, P.; Gao, J. Generalization of Block-Localized Wave Function for Constrained Optimization of Excited Determinants. *J. Chem. Theory Comput.* **2020**, *17*, 277–289.
- (43) Hait, D.; Head-Gordon, M. Highly Accurate Prediction of Core Spectra of Molecules at Density Functional Theory Cost: Attaining Sub-electronvolt Error from a Restricted Open-Shell Kohn–Sham Approach. *J. Phys. Chem. Lett.* **2020**, *11*, 775–786.
- (44) Hait, D.; Haugen, E. A.; Yang, Z.; Oosterbaan, K. J.; Leone, S. R.; Head-Gordon, M. Accurate prediction of core-level spectra of radicals at density functional theory cost via square gradient minimization and recoupling of mixed configurations. *J. Chem. Phys.* **2020**, *153*, 134108.
- (45) Garner, S. M.; Neuscammen, E. Core excitations with excited state mean field and perturbation theory. *J. Chem. Phys.* **2020**, *153*, 154102.
- (46) Zhao, R.; Grofe, A.; Wang, Z.; Bao, P.; Chen, X.; Liu, W.; Gao, J. Dynamic-then-static approach for core excitations of open-shell molecules. *J. Phys. Chem. Lett.* **2021**, *12*, 7409–7417.
- (47) Kahk, J. M.; Michelitsch, G. S.; Maurer, R. J.; Reuter, K.; Lischner, J. Core Electron Binding Energies in Solids from Periodic All-Electron Δ -Self-Consistent-Field Calculations. *J. Phys. Chem. Lett.* **2021**, *12*, 9353–9359.
- (48) Sun, J.; Ruzsinszky, A.; Perdew, J. P. Strongly Constrained and Appropriately Normed Semilocal Density Functional. *Phys. Rev. Lett.* **2015**, *115*, 036402.
- (49) Kahk, J. M.; Lischner, J. Accurate absolute core-electron binding energies of molecules, solids, and surfaces from first-principles calculations. *Phys. Rev. Mat.* **2019**, *3*, 100801.
- (50) Takahashi, O. Relativistic corrections for single- and double-core excitation at the K- and L-edges from Li to Kr. *Comput. Theor. Chem.* **2017**, *1102*, 80–86.

- (51) Norman, P.; Dreuw, A. Simulating X-ray spectroscopies and calculating core-excited states of molecules. *Chem. Rev.* **2018**, *118*, 7208–7248.
- (52) Bussy, A.; Hutter, J. Efficient and low-scaling linear-response time-dependent density functional theory implementation for core-level spectroscopy of large and periodic systems. *Phys. Chem. Chem. Phys.* **2021**, *23*, 4736–4746.
- (53) Stetina, T. F.; Kasper, J. M.; Li, X. Modeling L2, 3-edge X-ray absorption spectroscopy with linear response exact two-component relativistic time-dependent density functional theory. *J. Chem. Phys.* **2019**, *150*, 234103.
- (54) Repisky, M.; Konecny, L.; Kadek, M.; Komorovsky, S.; Malkin, O. L.; Malkin, V. G.; Ruud, K. Excitation energies from real-time propagation of the four-component Dirac–Kohn–Sham equation. *J. Chem. Theory Comput.* **2015**, *11*, 980–991.
- (55) Liu, J.; Cheng, L. Relativistic coupled-cluster and equation-of-motion coupled-cluster methods. *WIREs Comput. Mol. Sci.* **2021**, e1536.
- (56) Halbert, L.; Vidal, M. L.; Shee, A.; Coriani, S.; Severo Pereira Gomes, A. Relativistic EOM-CCSD for Core-Excited and Core-Ionized State Energies Based on the Four-Component Dirac–Coulomb (- Gaunt) Hamiltonian. *J. Chem. Theory Comput.* **2021**, *17*, 3583–3598.
- (57) Dyall, K. G. Interfacing relativistic and nonrelativistic methods. I. Normalized elimination of the small component in the modified Dirac equation. *J. Chem. Phys.* **1997**, *106*, 9618–9626.
- (58) Kutzelnigg, W.; Liu, W. Quasirelativistic theory equivalent to fully relativistic theory. *J. Chem. Phys.* **2005**, *123*, 241102.
- (59) Ilias, M.; Saue, T. An Infinite-Order Relativistic Hamiltonian by a Simple One-Step Transformation. *J. Chem. Phys.* **2007**, *126*, 064102.

- (60) Liu, W.; Peng, D. Exact Two-component Hamiltonians Revisited. *J. Chem. Phys.* **2009**, *131*, 031104.
- (61) Saue, T. Relativistic Hamiltonians for Chemistry: A Primer. *Chem. Phys. Chem.* **2011**, *12*, 3077–3094.
- (62) Li, Z.; Xiao, Y.; Liu, W. On the spin separation of algebraic two-component relativistic Hamiltonians. *J. Chem. Phys.* **2012**, *137*, 154114.
- (63) Cheng, L.; Gauss, J. Analytic energy gradients for the spin-free exact two-component theory using an exact block diagonalization for the one-electron Dirac Hamiltonian. *J. Chem. Phys.* **2011**, *135*, 084114.
- (64) Verma, P.; Derricotte, W. D.; Evangelista, F. A. Predicting near edge X-ray absorption spectra with the spin-free exact-two-component Hamiltonian and orthogonality constrained density functional theory. *J. Chem. Theory Comput.* **2016**, *12*, 144–156.
- (65) Kohn, W.; Sham, L. J. Self-consistent equations including exchange and correlation effects. *Phys. Rev.* **1965**, *140*, A1133–A1138.
- (66) Bagus, P. S. Self-consistent-field wave functions for hole states of some Ne-like and Ar-like ions. *Phys. Rev.* **1965**, *139*, A619–A634.
- (67) Ziegler, T.; Rauk, A.; Baerends, E. J. On the calculation of multiplet energies by the Hartree-Fock-Slater method. *Theor. Chim. Acta.* **1977**, *43*, 261–271.
- (68) Niskanen, J.; Norman, P.; Aksela, H.; Ågren, H. Relativistic contributions to single and double core electron ionization energies of noble gases. *J. Chem. Phys.* **2011**, *135*, 054310.
- (69) Zheng, X.; Cheng, L. Performance of Delta-Coupled-Cluster Methods for Calculations of Core-Ionization Energies of First-Row Elements. *J. Chem. Theory Comput.* **2019**, *15*, 4945–4955.

- (70) Frank, I.; Hutter, J.; Marx, D.; Parrinello, M. Molecular dynamics in low-spin excited states. *J. Chem. Phys.* **1998**, *108*, 4060–4069.
- (71) Kowalczyk, T.; Tsuchimochi, T.; Chen, P.-T.; Top, L.; Van Voorhis, T. Excitation energies and Stokes shifts from a restricted open-shell Kohn-Sham approach. *J. Chem. Phys.* **2013**, *138*, 164101.
- (72) Ågren, H.; Nordgren, J.; Selander, L.; Nordling, C.; Siegbahn, K. Multiplet structure in the high-resolution x-ray emission spectrum of neon. *J. Electron Spectrosc. Relat. Phenom.* **1978**, *14*, 27–39.
- (73) Banna, M.; Wallbank, B.; Frost, D.; McDowell, C.; Perera, J. Free atom core binding energies from X-ray photoelectron spectroscopy. II. Na, K, Rb, Cs, and Mg. *J. Chem. Phys.* **1978**, *68*, 5459–5466.
- (74) Bodeur, S.; Millié, P.; Nenner, I. Single- and multiple-electron effects in the Si 1s photoabsorption spectra of SiX₄ (X= H, D, F, Cl, Br, CH₃, C₂H₅, OCH₃, OC₂H₅) molecules: Experiment and theory. *Phys. Rev. A* **1990**, *41*, 252–263.
- (75) Sodhi, R. N.; Cavell, R. G. KLL Auger and core-level (1s and 2p) photoelectron shifts in a series of gaseous phosphorus compounds. *J. Electron Spectrosc. Relat. Phenom.* **1983**, *32*, 283–312.
- (76) Keski-Rahkonen, O.; Krause, M. Energies and chemical shifts of the sulphur 1s level and the KL₂L₃ (¹D₂) Auger line in H₂S, SO₂ and SF₆. *J. Electron Spectrosc. Relat. Phenom.* **1976**, *9*, 371–380.
- (77) Perera, R. C.; LaVilla, R. E. Molecular x-ray spectra: S-K β emission and K absorption spectra of SCO and CS₂. *J. Chem. Phys.* **1984**, *81*, 3375–3382.
- (78) Sodhi, R. N.; Cavell, R. G. KLL auger and core level (1s and 2p) photoelectron shifts

- in a series of gaseous sulfur compounds. *J. Electron Spectrosc. Relat. Phenom.* **1986**, *41*, 1–24.
- (79) Bodeur, S.; Maréchal, J.; Reynaud, C.; Bazin, D.; Nenner, I. Chlorine K shell photoabsorption spectra of gas phase HCl and Cl₂ molecules. *Zeitschrift für Physik D Atoms, Molecules and Clusters* **1990**, *17*, 291–298.
- (80) Lindle, D. W.; Cowan, P.; Jach, T.; LaVilla, R.; Deslattes, R.; Perera, R. C. Polarized x-ray emission studies of methyl chloride and the chlorofluoromethanes. *Phys. Rev. A* **1991**, *43*, 2353–2366.
- (81) Reynaud, C.; Bodeur, S.; Maréchal, J.; Bazin, D.; Millié, P.; Nenner, I.; Rockland, U.; Baumgärtel, H. Electronic properties of the SF₅Cl molecule: a comparison with SF₆. I. Photoabsorption spectra near the sulphur K and chlorine K edges. *Chem. Phys.* **1992**, *166*, 411–424.
- (82) Breinig, M.; Chen, M. H.; Ice, G. E.; Parente, F.; Crasemann, B.; Brown, G. S. Atomic inner-shell level energies determined by absorption spectrometry with synchrotron radiation. *Phys. Rev. A* **1980**, *22*, 520–528.
- (83) Ambroise, M. A.; Jensen, F. Probing Basis Set Requirements for Calculating Core Ionization and Core Excitation Spectroscopy by the Δ Self-Consistent-Field Approach. *J. Chem. Theory Comput.* **2018**, *15*, 325–337.
- (84) Jensen, F. Unifying general and segmented contracted basis sets. Segmented polarization consistent basis sets. *J. Chem. Theory Comput.* **2014**, *10*, 1074–1085.
- (85) Becke, A. D. Density-functional thermochemistry. III. The role of exact exchange. *J. Chem. Phys.* **1993**, *98*, 5648–5652.
- (86) Stephens, P. J.; Devlin, F. J.; Chabalowski, C. F.; Frisch, M. J. Ab initio calculation

- of vibrational absorption and circular dichroism spectra using density functional force fields. *J. Phys. Chem.* **1994**, *98*, 11623–11627.
- (87) Adamo, C.; Barone, V. Toward reliable density functional methods without adjustable parameters: The PBE0 model. *J. Chem. Phys.* **1999**, *110*, 6158–6170.
- (88) Tao, J.; Perdew, J. P.; Staroverov, V. N.; Scuseria, G. E. Climbing the density functional ladder: Nonempirical meta-generalized gradient approximation designed for molecules and solids. *Phys. Rev. Lett.* **2003**, *91*, 146401.
- (89) Chan, B. Assessment and development of DFT with the expanded CUAGAU-2 set of group-11 cluster systems. *Int. J. Quantum Chem.* **2021**, *121*, e26453.
- (90) Hui, K.; Chai, J.-D. SCAN-based hybrid and double-hybrid density functionals from models without fitted parameters. *J. Chem. Phys.* **2016**, *144*, 044114.
- (91) Becke, A. D. A new mixing of Hartree–Fock and local density-functional theories. *J. Chem. Phys.* **1993**, *98*, 1372–1377.
- (92) Perdew, J. P.; Burke, K.; Ernzerhof, M. Generalized gradient approximation made simple. *Phys. Rev. Lett.* **1996**, *77*, 3865–3868.
- (93) Cavell, R. G.; Jürgensen, A. Chemical shifts in P-1s photoabsorption spectra of gaseous phosphorus compounds. *J. Electron Spectrosc. Relat. Phenom.* **1999**, *101*, 125–129.
- (94) Reynaud, C.; Gaveau, M.-A.; Bisson, K.; Millié, P.; Nenner, I.; Bodeur, S.; Archirel, P.; Lévy, B. Double-core ionization and excitation above the sulphur K-edge in H₂S, SO₂ and SF₆. *J. Phys. B: At. Mol. Opt. Phys.* **1996**, *29*, 5403–5419.
- (95) Bodeur, S.; Hitchcock, A. Inner-and valence-shell excitation of SF₄ studied by photoabsorption and electron energy loss spectroscopy. *Chem. Phys.* **1987**, *111*, 467–479.
- (96) Evangelista, F. A.; Shushkov, P.; Tully, J. C. Orthogonality constrained density functional theory for electronic excited states. *J. Phys. Chem. A* **2013**, *117*, 7378–7392.

- (97) Woon, D. E.; Dunning Jr, T. H. Gaussian basis sets for use in correlated molecular calculations. V. Core-valence basis sets for boron through neon. *J. Chem. Phys.* **1995**, *103*, 4572–4585.
- (98) Mennucci, B. Polarizable continuum model. *Wiley Interdiscip. Rev. Comput. Mol. Sci.* **2012**, *2*, 386–404.
- (99) Cancès, E.; Mennucci, B.; Tomasi, J. A new integral equation formalism for the polarizable continuum model: Theoretical background and applications to isotropic and anisotropic dielectrics. *J. Chem. Phys.* **1997**, *107*, 3032–3041.
- (100) Kunze, L.; Hansen, A.; Grimme, S.; Mewes, J.-M. PCM-ROKS for the Description of Charge-Transfer States in Solution: Singlet–Triplet Gaps with Chemical Accuracy from Open-Shell Kohn–Sham Reaction-Field Calculations. *J. Phys. Chem. Lett.* **2021**, *12*, 8470–8480.
- (101) Sutherland, D.; Kasrai, M.; Bancroft, G.; Liu, Z.; Tan, K. Si L- and K-edge x-ray-absorption near-edge spectroscopy of gas-phase $\text{Si}(\text{CH}_3)_x(\text{OCH}_3)_{4-x}$: Models for solid-state analogs. *Phys. Rev. B* **1993**, *48*, 14989–15001.
- (102) Engemann, C.; Kohring, G.; Pantelouris, A.; Hormes, J.; Grimme, S.; Peyerimhoff, S.; Clade, J.; Frick, F.; Jansen, M. Experimental and theoretical investigations of the X-ray absorption near edge spectra (XANES) of P_4O_6 and $\text{P}_4\text{O}_6\text{X}$ ($\text{X} = \text{O}, \text{S}, \text{Se}$). *Chem. Phys.* **1997**, *221*, 189–198.
- (103) Ibuki, T.; Shimada, Y.; Nagaoka, S.; Fujii, A.; Hino, M.; Kakiuchi, T.; Okada, K.; Tabayashi, K.; Matsudo, T.; Yamana, Y. et al. Total photoabsorption cross-sections of CF_3SF_5 in the C, F and S K-shell regions. *Chem. Phys. Lett.* **2004**, *392*, 303–308.
- (104) Ochmann, M.; Hussain, A.; Von Ahnen, I.; Cordones, A. A.; Hong, K.; Lee, J. H.; Ma, R.; Adamczyk, K.; Kim, T. K.; Schoenlein, R. W. et al. UV-photochemistry of the

- disulfide bond: Evolution of early photoproducts from picosecond X-ray absorption spectroscopy at the sulfur K-Edge. *J. Am. Chem. Soc.* **2018**, *140*, 6554–6561.
- (105) DeBeer George, S.; Brant, P.; Solomon, E. I. Metal and ligand K-Edge XAS of organotitanium complexes: Metal 4p and 3d contributions to pre-edge intensity and their contributions to bonding. *J. Am. Chem. Soc.* **2005**, *127*, 667–674.
- (106) McKeown, D. A.; Gan, H.; Pegg, I. L.; Stolte, W. C.; Demchenko, I. X-ray absorption studies of chlorine valence and local environments in borosilicate waste glasses. *J. Nuc. Mat.* **2011**, *408*, 236–245.
- (107) Shadle, S. E.; Hedman, B.; Hodgson, K. O.; Solomon, E. I. Ligand K-edge X-ray absorption spectroscopic studies: metal-ligand covalency in a series of transition metal tetrachlorides. *J. Am. Chem. Soc.* **1995**, *117*, 2259–2272.
- (108) Thom, A. J.; Head-Gordon, M. Hartree–Fock solutions as a quasidiabatic basis for nonorthogonal configuration interaction. *J. Chem. Phys.* **2009**, *131*, 124113.
- (109) List, N. H.; Melin, T. R. L.; van Horn, M.; Saue, T. Beyond the electric-dipole approximation in simulations of x-ray absorption spectroscopy: Lessons from relativistic theory. *J. Chem. Phys.* **2020**, *152*, 184110.
- (110) Rees, J. A.; Wandzilak, A.; Maganas, D.; Wurster, N. I.; Hugenbruch, S.; Kowalska, J. K.; Pollock, C. J.; Lima, F. A.; Finkelstein, K. D.; DeBeer, S. Experimental and theoretical correlations between vanadium K-edge X-ray absorption and $K\beta$ emission spectra. *J. Bio. Inor. Chem.* **2016**, *21*, 793–805.
- (111) Farges, F. Chromium speciation in oxide-type compounds: application to minerals, gems, aqueous solutions and silicate glasses. *Phys. Chem. Minerals* **2009**, *36*, 463–481.
- (112) Hall, E. R.; Pollock, C. J.; Bendix, J.; Collins, T. J.; Glatzel, P.; DeBeer, S. Valence-

- to-core-detected X-ray absorption spectroscopy: Targeting ligand selectivity. *J. Am. Chem. Soc.* **2014**, *136*, 10076–10084.
- (113) Lancaster, K. M.; Finkelstein, K. D.; DeBeer, S. $K\beta$ X-ray emission spectroscopy offers unique chemical bonding insights: revisiting the electronic structure of ferrocene. *Inorg. Chem.* **2011**, *50*, 6767–6774.
- (114) Liu, W.; Borg, S. J.; Testemale, D.; Etschmann, B.; Hazemann, J.-L.; Brugger, J. Speciation and thermodynamic properties for cobalt chloride complexes in hydrothermal fluids at 35–440 C and 600 bar: an in-situ XAS study. *Geochim. Cosmochim. Acta* . **2011**, *75*, 1227–1248.
- (115) DiMucci, I. M.; Lukens, J. T.; Chatterjee, S.; Carsch, K. M.; Titus, C. J.; Lee, S. J.; Nordlund, D.; Betley, T. A.; MacMillan, S. N.; Lancaster, K. M. The myth of d^8 copper (III). *J. Am. Chem. Soc.* **2019**, *141*, 18508–18520.
- (116) Balabanov, N. B.; Peterson, K. A. Systematically convergent basis sets for transition metals. I. All-electron correlation consistent basis sets for the 3d elements Sc–Zn. *J. Chem. Phys.* **2005**, *123*, 064107.
- (117) Yamamoto, T. Assignment of pre-edge peaks in K-edge x-ray absorption spectra of 3d transition metal compounds: electric dipole or quadrupole? *X-Ray Spectrom.* **2008**, *37*, 572–584.
- (118) Southworth, S. H.; Dunford, R. W.; Ray, D.; Kanter, E. P.; Doumy, G.; March, A. M.; Ho, P. J.; Krässig, B.; Gao, Y.; Lehmann, C. S. et al. Observing pre-edge K -shell resonances in Kr, Xe, and XeF₂. *Phys. Rev. A* **2019**, *100*, 022507.
- (119) Breit, G. Dirac’s equation and the spin-spin interactions of two electrons. *Phys. Rev.* **1932**, *39*, 616–624.

- (120) Koziol, K.; Aucar, G. A. QED effects on individual atomic orbital energies. *J. Chem. Phys.* **2018**, *148*, 134101.
- (121) Szabo, A.; Ostlund, N. S. *Modern Quantum Chemistry: Introduction to Advanced Electronic Structure Theory*; Dover Publications, Inc.: Mineola, New York, 1996; pp 286–296.
- (122) Zheng, X.; Zhang, C.; Jin, Z.; Southworth, S. H.; Cheng, L. Benchmark Relativistic Delta-Coupled-Cluster Calculations of K-Edge Core-Ionization Energies for Third-Row Elements. *Phys. Chem. Chem. Phys.* **2022**, *Submitted*.
- (123) Wen, A.; Hitchcock, A. Inner shell spectroscopy of $(\eta^5\text{-C}_5\text{H}_5)_2\text{TiCl}_2, (\eta^5\text{-C}_5\text{H}_5)\text{TiCl}_3$, and TiCl_4 . *Can. J. Chem.* **1993**, *71*, 1632–1644.
- (124) Mitzner, R.; Rehanek, J.; Kern, J.; Gul, S.; Hattne, J.; Taguchi, T.; Alonso-Mori, R.; Tran, R.; Weniger, C.; Schröder, H. et al. L-edge x-ray absorption spectroscopy of dilute systems relevant to metalloproteins using an x-ray free-electron laser. *J. Phys. Chem. Lett.* **2013**, *4*, 3641–3647.
- (125) Hocking, R. K.; Wasinger, E. C.; de Groot, F. M.; Hodgson, K. O.; Hedman, B.; Solomon, E. I. Fe L-edge XAS studies of $\text{K}_4[\text{Fe}(\text{CN})_6]$ and $\text{K}_3[\text{Fe}(\text{CN})_6]$: a direct probe of back-bonding. *J. Am. Chem. Soc.* **2006**, *128*, 10442–10451.
- (126) Wen, A.; Rühl, E.; Hitchcock, A. Inner-shell excitation of organoiron compounds by electron impact. *Organometallics* **1992**, *11*, 2559–2569.
- (127) Epifanovsky, E., et al. Software for the frontiers of quantum chemistry: An overview of developments in the Q-Chem 5 package. *J. Chem. Phys.* **2021**, *155*, 084801.
- (128) Perdew, J. P.; Parr, R. G.; Levy, M.; Balduz Jr, J. L. Density-functional theory for fractional particle number: derivative discontinuities of the energy. *Phys. Rev. Lett.* **1982**, *49*, 1691–1694.

- (129) Hait, D.; Head-Gordon, M. Delocalization errors in density functional theory are essentially quadratic in fractional occupation number. *J. Phys. Chem. Lett.* **2018**, *9*, 6280–6288.
- (130) Sun, Q.; Zhang, X.; Banerjee, S.; Bao, P.; Barbry, M.; Blunt, N. S.; Bogdanov, N. A.; Booth, G. H.; Chen, J.; Cui, Z.-H. et al. Recent developments in the PySCF program package. *J. Chem. Phys.* **2020**, *153*, 024109.
- (131) Johnson III, R. D. NIST Computational Chemistry Comparison and Benchmark Database, NIST Standard Reference Database Number 101, Release 18. October 2016. *NIST* **2015**,
- (132) Groom, C. R.; Bruno, I. J.; Lightfoot, M. P.; Ward, S. C. The Cambridge structural database. *Acta Crystallogr. B: Struct. Sci., Cryst. Eng. Mater.* **2016**, *72*, 171–179.
- (133) Mardirossian, N.; Head-Gordon, M. ω B97M-V: A combinatorially optimized, range-separated hybrid, meta-GGA density functional with VV10 nonlocal correlation. *J. Chem. Phys.* **2016**, *144*, 214110.
- (134) McGinney, J. A. Cesium tetrachlorocuprate. Structure, crystal forces, and charge distribution. *J. Am. Chem. Soc.* **1972**, *94*, 8406–8413.
- (135) Franck, J.; Dymond, E. Elementary processes of photochemical reactions. *Trans. Far. Soc.* **1926**, *21*, 536–542.
- (136) Condon, E. A theory of intensity distribution in band systems. *Phys. Rev.* **1926**, *28*, 1182–1201.
- (137) Kutzelnigg, W. Basis set expansion of the Dirac operator without variational collapse. *Int. J. Quantum Chem.* **1984**, *25*, 107–129.
- (138) Smith, D. G.; Burns, L. A.; Simmonett, A. C.; Parrish, R. M.; Schieber, M. C.; Galvelis, R.; Kraus, P.; Kruse, H.; Di Remigio, R.; Alenaizan, A. et al. PSI4 1.4:

- Open-source software for high-throughput quantum chemistry. *J. Chem. Phys.* **2020**, *152*, 184108.
- (139) Carroll, T. X.; Ji, D.; Maclaren, D. C.; Thomas, T. D.; Saethre, L. J. Relativistic corrections to reported sulfur 1s ionization energies. *J. Electron Spectrosc. Relat. Phenom.* **1987**, *42*, 281–284.
- (140) Cavell, R.; Sodhi, R. The effect of relativistic curvature calibration corrections for a non-retarding hemispherical sector analyzer: revision of the absolute S1s binding energy of H₂S and the KLL auger energy of PH₃. *J. Electron Spectrosc. Relat. Phenom.* **1987**, *43*, 215–223.
- (141) Bourne Worster, S.; Feighan, O.; Manby, F. R. Reliable transition properties from excited-state mean-field calculations. *J. Chem. Phys.* **2021**, *154*, 124106.